CAMERA CALIBRATION FROM A TRANSLATION + PLANAR MOTION

Hui Zhang, Kwan-Yee Kenneth Wong
Department of Computer Science, The University of Hong Kong, Pokfulam Rd, Hong Kong
{hzhang, kykwong}@cs.hku.hk

ABSTRACT
This paper addresses the problem of camera calibration by exploiting image invariants under camera/object rotation. A novel translation + planar motion is studied here. The 3×3 homography mapping corresponding points before and after the motion is exploited to obtain image invariants under perspective projection. The homography is found to form a "rotation conic" under different rotation angles. Apart from the imaged circular points, this conic can also be exploited to find the vanishing point of the rotation axis and this provides extra constraints for camera calibration. A square calibration pattern, which is invariant under a rotation about its center by multiples of $\pi/2$ radians, is introduced as a special instantiation of the translation + planar motion. Experiments on synthetic and real data show good precisions in calibration results.
KEY WORDS
Camera calibration, translation, planar motion.

1 Introduction

Camera calibration, the determination of the camera intrinsic parameters, is traditionally achieved by imaging some special objects with known metric structure [1][2][3]. Self-calibration, on the other hand, relies only on scene rigidity to estimate the camera intrinsics [4]. Between these two extremes, there are also a number of calibration techniques developed for constrained motions, e.g., pure rotation [5], planar motion [6], etc. Knowledge about the scene or motion often results in faster, more flexible, or more accurate calibration. Compared with pure rotation, planar motion provides less strong matching constraints, yet it is more flexible by allowing an additional translational component in the motion. Note rotation exists in both these motions, from which the pair of imaged circular points of the scene plane can be obtained for calibration. Similar example also includes circular motion [7].

Inspired by the studies on planar motion [6] and circular motion [7], a translation + planar motion is considered here for camera calibration. Such a motion allows an arbitrary translation of a planar patch followed by a motion on the patch plane. Such a motion can be screw decomposed into a planar rotation about a screw axis and a translation along the screw axis. This paper first exploits the homography relating corresponding points on two circles to recover some image invariants, then extends to the case of any planar patches under a translation + planar motion. A "*rotation conic*" is found from the eigenvectors of the homography mapping corresponding points before and after the motion by changing the planar rotation angles. Note this rotation conic is different from the conic described in [8], which can be regarded as images of a sphere. The imaged circular points are found to lie on this rotation conic. Furthermore, the vanishing point of the screw axis can be obtained from the intersection between the rotation conic and the image of the screw axis. In this way, the image invariants under such a motion are fully exploited, and thus improves the calibration precision and reduces the number of additional motions needed for calibration. There can be various instantiations of the above theory. Note if the translation becomes zero, this motion degenerates to a planar rotation by skew decomposition, and the rotation conic become a family of conics passing through the skew center and the two circular points. A special square calibration pattern is then introduced to illustrate the proposed approach. Good precision in the experimental results shows the practicality of the proposed method.

This paper is organized as follows. Section 2 presents the theoretical background for camera calibration from the absolute conic. By studying the eigenvectors of the homography relating two conics, Section 3 first derives the rotation conic and the invariants useful in camera calibration, then extends the ideas to the translation + planar motion. In Section 4, square patterns are introduced for camera calibration. Results of synthetic and real data experiments are presented in Section 5. Conclusions are given in Section 6.

2 Theoretical Background

2.1 Calibration with the absolute conic

The absolute conic was first introduced by Faugeras et al. [9]. It is a point conic on the plane at infinity $\mathbf{\Pi}_\infty$ that is invariant to rotation and translation as a set. It projects to the image of the absolute conic (IAC) as

$$\boldsymbol{\omega} = \mathbf{K}^{-\mathbf{T}}\mathbf{K}^{-\mathbf{1}}. \tag{1}$$

Here $\mathbf{K}$ is the camera intrinsic matrix and is defined as

$$\mathbf{K} = \begin{bmatrix} \alpha f & s & u_0 \\ 0 & f & v_0 \\ 0 & 0 & 1 \end{bmatrix}, \tag{2}$$

where f is the focal length, α is the aspect ratio, (u_0, v_0) is the principal point and s is the skew.

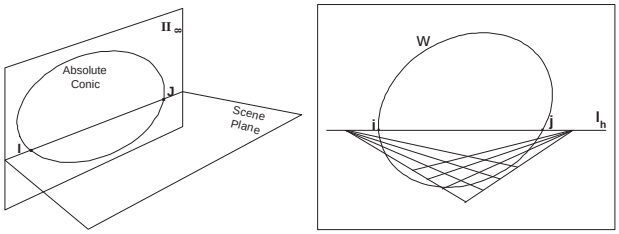

(a) (b)

Figure 1. Projection invariants for camera calibration. **(a)** In 3D space, the circular points are the complex intersection points of the scene plane with the absolute conic. **(b)** In 2D image, the intersecting relationship preserves.

The image of the absolute conic, and its dual (DIAC) $\omega^* = \mathbf{K}\mathbf{K}^\mathbf{T}$ [10], are the 2D projections of the 3D invariant absolute conic (AC) and the dual of the absolute conic (DAC), respectively. The IAC and DIAC are imaginary point and line conics respectively. The camera calibration matrix $\mathbf{K}$ can be easily obtained from the IAC or DIAC by Cholesky decomposition [11]. Note when skew $s = 0$, the camera is a *zero skew* camera. When the aspect ratio is also known to be unity, the camera is then called a *natural camera*.

The image of the absolute conics can generally be found by making use of the following constraints:

- **Circular points** The circular points $\mathbf{I}$ and $\mathbf{J}$ are the complex intersection points of the scene plane with the absolute conic in $\mathbf{\Pi}_\infty$ (see Fig.1(a)). The images $\mathbf{i}$ and $\mathbf{j}$ of this pair of circular points lie on the ω (see Fig.1(b)), and hence

$$\mathbf{i}^\mathbf{T}\omega\mathbf{i} = 0 \quad \text{and} \quad \mathbf{j}^\mathbf{T}\omega\mathbf{j} = 0, \tag{3}$$

$$\mathbf{l}_h = \mathbf{i} \times \mathbf{j}, \tag{4}$$

  where $\mathbf{l}_h$ is the image of the intersection line between the scene plane and $\mathbf{\Pi}_\infty$ (i.e. the horizon). Five or more circular points are sufficient to estimate the IAC ω, and hence $\mathbf{K}$. A minimal number of four circular points is required to calibrate a zero skew camera or at least three such points for calibrating a natural camera. The accuracy is reliant on obtaining as many images as possible from widely separated viewpoints.

- **Orthogonality** The vanishing point $\mathbf{v}$ of the normal direction to a plane and the vanishing line $\mathbf{l}$ of the plane are the pole and polar w.r.t. the ω [10], i.e.,

$$\mathbf{l} = \omega\mathbf{v}. \tag{5}$$

  Thus to fully calibrate a camera, at least three such conjugate pairs are needed. To calibrate a zero skew /natural camera, at least two pairs are needed. Note these constraints, together with the constraints from circular points, can be used in camera calibration simultaneously.

3 Calibration from Homography

3.1 Homography Relating Two Conics

Consider an arbitrary pinhole camera $\mathbf{P}$ viewing two sets of points on two rotating concentric circles with a displacement parallel to the plane normal.

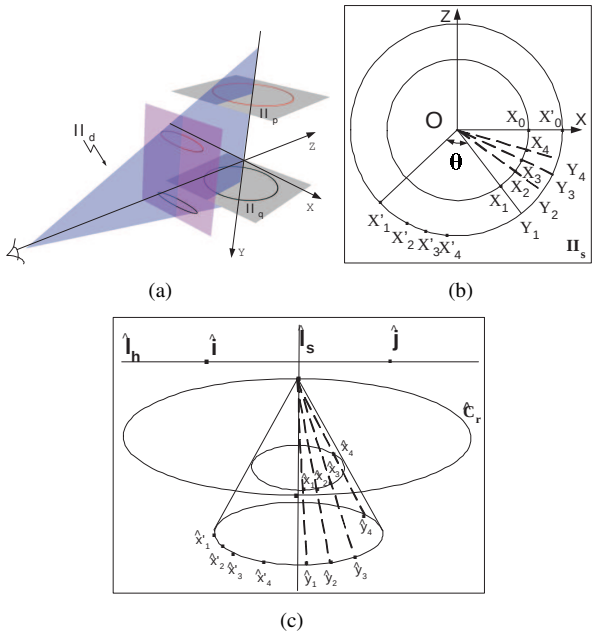

(a) (b)

(c)

Figure 2. The perspective projection. **(a)** A pinhole camera $\hat{\mathbf{P}}$ is viewing two sets of points on two concentric circles. **(b)** Top view of the two point sets lying on two circles of different planes. **(c)** The circular points and the rotation conic can be obtained from the homography relating the two point sets $\hat{\mathbf{x}}_i$ and $\hat{\mathbf{x}}'_i$.

Theorem I. *By varying the rotation angle, the eigenvectors of the homography relating the images of the two parallel circles trace out a conic, termed as the rotation conic.*

Proof. Let's consider a camera $\hat{\mathbf{P}} = [\mathbf{I}_3|\mathbf{c}]$ centered at $-\mathbf{c} = [0\,0\,d_z]^\mathbf{T}$, with $d_z > 0$, viewing two sets of points on two concentric rotating circles, whose rotation axis coincides with the Y-axis (see Fig.2(a)). The plane $\mathbf{\Pi}_d$ contains the Y-axis and the camera center, with its normal direction $\mathbf{N}_x = [1\,0\,0\,0]^\mathbf{T}$. Let $\mathbf{X}_0 = [X_0\,Y_0\,0\,1]^\mathbf{T}$ and $\mathbf{X}'_0 = [X'_0\,Y'_0\,0\,1]^\mathbf{T}$ be the generating points of the two circles (see Fig.2(b)), ϕ_i be the absolute rotation angles for the points $\mathbf{X}_i$ and $\mathbf{X}'_i$ $(i = 1, ..., 4)$ measured from the positive X-axis, and θ be the relative rotation angle between the two point sets.

The images $\hat{\mathbf{x}}_i$, $\hat{\mathbf{x}}'_i$ (see Fig.2(c)) of the points $\mathbf{X}_i$, $\mathbf{X}'_i$ $(i = 1, ..., 4)$ under $\hat{\mathbf{P}}$ are given by

$$\hat{\mathbf{x}}_i = [\mathbf{I}|\mathbf{c}] \begin{bmatrix} X_0 cos\phi_i \\ Y_0 \\ X_0 sin\phi_i \\ 1 \end{bmatrix} = \begin{bmatrix} X_0 & 0 & 0 \\ 0 & 0 & Y_0 \\ 0 & X_0 & d_z \end{bmatrix} \begin{bmatrix} cos\phi_i \\ sin\phi_i \\ 1 \end{bmatrix},$$

$$\hat{\mathbf{x}}'_i = [\mathbf{I}|\mathbf{c}] \begin{bmatrix} X'_0 cos(\phi_i+\theta) \\ Y'_0 \\ X'_0 sin(\phi_i+\theta) \\ 1 \end{bmatrix} = \begin{bmatrix} X'_0 cos\theta & -X'_0 sin\theta & 0 \\ 0 & 0 & Y'_0 \\ X'_0 sin\theta & X'_0 cos\theta & d_z \end{bmatrix} \begin{bmatrix} cos\phi_i \\ sin\phi_i \\ 1 \end{bmatrix}.$$

Hence $\hat{\mathbf{x}}'$ and $\hat{\mathbf{x}}$ are related by a homography $\hat{\mathbf{H}}(\theta)$, where

$$\hat{\mathbf{H}}(\theta) = \begin{bmatrix} \frac{X'_0 cos\theta}{X_0} & \frac{-d_z X'_0 sin\theta}{X_0 Y_0} & \frac{-X'_0 sin\theta}{X_0} \\ 0 & \frac{Y'_0}{Y_0} & 0 \\ \frac{X'_0 sin\theta}{X_0} & \frac{-d_z X'_0 cos\theta}{X_0 Y_0} + \frac{d_z}{Y_0} & \frac{X'_0 cos\theta}{X_0} \end{bmatrix}. \quad (6)$$

The eigenvectors of $\hat{\mathbf{H}}(\theta)$ can be found from $\hat{\mathbf{H}}(\theta)\mathbf{e} = \lambda\mathbf{e}$. By representing the coordinates of the eigenvector $\mathbf{e}$ in terms of the rotation angle θ and then eliminating θ, a conic can be obtained as

$$\hat{\mathbf{C}}_r = \begin{bmatrix} X_0^2 Y_0'^2 - X_0'^2 Y_0^2 & 0 & 0 \\ 0 & d_z^2(X_0^2 - X_0'^2) & d_z(X_0'^2 Y_0 - X_0^2 Y_0') \\ 0 & d_z(X_0'^2 Y_0 - X_0^2 Y_0') & X_0^2 Y_0'^2 - X_0'^2 Y_0^2 \end{bmatrix}. \quad (7)$$

In this paper, this conic is termed as the "*rotation conic*" and each point on it corresponds to a single rotation angle θ (see Fig.2(c)).

Let $\hat{\mathbf{l}}_h = [0\,1\,0]^{\mathbf{T}}$ be the horizon of the X-Z plane. It intersects $\hat{\mathbf{C}}_r$ at two complex points $\hat{\mathbf{i}}, \hat{\mathbf{j}} = [1\,0\,\pm i]^{\mathbf{T}}$ which are the images of the circular points $[1\,0\,\pm i\,0]^{\mathbf{T}}$ of the X-Z plane. Hence $\hat{\mathbf{C}}_r$ implicitly contains the pair of imaged circular points. Furthermore, let $\hat{\mathbf{l}}_s = [1\,0\,0]^{\mathbf{T}}$ be the image of the rotation axis and $\hat{\mathbf{v}}_x = [1\,0\,0]^{\mathbf{T}}$ the vanishing point associated with $\mathbf{N}_x$, it can be shown that $\hat{\mathbf{l}}_s = \hat{\mathbf{C}}_r\hat{\mathbf{v}}_x$, i.e. $\hat{\mathbf{v}}_x$ and $\hat{\mathbf{l}}_s$ are conjugate w.r.t. $\hat{\mathbf{C}}_r$. The two intersection points between $\hat{\mathbf{C}}_r$ and $\hat{\mathbf{l}}_s$ are the imaged vertexes of the 3D cones with sections being the two circles. If the two circles are of the same radius (i.e. $X_0 = X'_0$), $\hat{\mathbf{C}}_r$ becomes a parabola which intersects $\hat{\mathbf{l}}_s$ at $[0\ \frac{Y_0+Y'_0}{2d_z}\ 1]^{\mathbf{T}}$ and the vanishing point $\mathbf{v}_y = [0\,1\,0]^{\mathbf{T}}$ of the Y-axis. When the two point sets lie on the same plane (i.e. $Y_0 = Y'_0$), $\hat{\mathbf{C}}_r$ becomes a family of conics passing through the image of the concentric circle center $[0\,Y_0/d_z\,1]^{\mathbf{T}}$ and the two imaged circular points $\hat{\mathbf{i}}$,$\hat{\mathbf{j}}$.

Now consider an arbitrary pinhole camera $\mathbf{P} = \mathbf{KR}[\mathbf{I}|\mathbf{c}]$ which is defined by applying a rotation $\mathbf{R}$ and a camera calibration matrix $\mathbf{K}$ to $\hat{\mathbf{P}}$. Let the planar homography $\mathbf{H}_r = \mathbf{KR}$ transforms the image formed by $\hat{\mathbf{P}}$ into the image formed by $\mathbf{P}$. Thus the homography relating $\mathbf{x} = \mathbf{H_r}\hat{\mathbf{x}}$ to $\mathbf{x}' = \mathbf{H_r}\hat{\mathbf{x}}'$ is given by $\mathbf{H}(\theta) = \mathbf{H}_r\hat{\mathbf{H}}(\theta)\mathbf{H}_r^{-1}$, and the rotation conic under $\mathbf{P}$ is given by $\mathbf{C}_r = \mathbf{H}_r^{-T}\hat{\mathbf{C}}_r\mathbf{H}_r^{-1}$. $\mathbf{C}_r$ has the similar properties as $\hat{\mathbf{C}}_r$:

- Each point on $\mathbf{C}_r$ corresponds to one rotation angle θ.
- $\mathbf{C}_r$ intersects with the horizon $\mathbf{l}_h = \mathbf{H}_r^{-\mathbf{T}}\hat{\mathbf{l}}_h$ at the images of the two circular points $\mathbf{i} = \mathbf{H}_r\hat{\mathbf{i}}$, $\mathbf{j} = \mathbf{H}_r\hat{\mathbf{j}}$.
- The vanishing point $\mathbf{v}_x = \mathbf{H}_r\hat{\mathbf{v}}_x$ and the rotation axis $\mathbf{l}_s = \mathbf{H}_r^{-\mathbf{T}}\hat{\mathbf{l}}_s$ are conjugate w.r.t. $\mathbf{C}_r$, i.e., $\mathbf{l}_s = \mathbf{C}_r\mathbf{v}_x$.
- The two intersection points between $\mathbf{C}_r$ and $\mathbf{l}_s$ are the images of the outer and inner vertexes of the cones formed from the two circles. If $X_0 = X'_0$, the outer vertex is the vanishing point $\mathbf{v}_y$ of rotation axis.
- If the two point sets are co-planar (i.e. $Y_0 = Y'_0$), $\mathbf{C}_r$ becomes a family of conics passing through the image of the circle center and $\mathbf{i}$,$\mathbf{j}$.

$\mathbf{C}_r$ can thus provide four independent constraints on the IAC from $\mathbf{i}$, $\mathbf{j}$, the conjugate pairs of $\mathbf{l}_h$, $\mathbf{v}_y$ and $\mathbf{l}_s$, $\mathbf{v}_x$. Hence the camera can be fully calibrated from at least two different rotation conics, and a zero skew/natual camera can be calibrated from only one.

3.2 Extension to translation + planar Motion

The derived rotation conic and its properties can be extended to point sets on two planar patches. The homography relating two circles has another unique decomposition, given by [7]

$$\mathbf{H}(\theta) = \mathbf{H}_{qs}^{-1}\mathbf{R}(\theta)\mathbf{H}_{qs}\mathbf{H}_{pq}, \quad (8)$$

where $\mathbf{H}_{pq}$ is the planar homology relating the points $\mathbf{x}_i$ lying on the plane Π_p to those points $\mathbf{y}_i (i = 1,2,3,4)$ on Π_q (see Fig.3(c)), which are not constraint on circles. $\mathbf{H}_{pq}$ is defined by

$$\mathbf{H}_{pq} = \mathbf{I} + (\mu - 1)\frac{\mathbf{v}\mathbf{l}_h^{\mathbf{T}}}{\mathbf{v}^{\mathbf{T}}\mathbf{l}_h}, \quad (9)$$

which has a line of fixed points $\mathbf{l}_h$(axis) and a fixed point $\mathbf{v}$ (vertex) not on the axis[10]. Its eigenvalues are, up to a common scalar, $(\mu, 1, 1)$. Among its three eigenvectors, the one corresponding to μ is the vertex $\mathbf{v}$ and the other two span the axis $\mathbf{l}_h$. In (8), $\mathbf{H}_{qs}$ is the homography mapping the points on the plane $\mathbf{\Pi}_q$ to the points on a reference plane Π_s. $\mathbf{R}(\theta)$ is the rotation matrix relating the points $\mathbf{Y}_i$ to $\mathbf{X}'_i (i = 1,2,3,4)$ (see Fig.3(b)), whose eigenvalues are $(1, e^{i\theta}, e^{-i\theta})$ and the corresponding eigenvectors are the direction of the rotation axis (i.e. Y-axis) and the two circular points $[1\ \pm i\,0]^{\mathbf{T}}$ of the parallel planes $\mathbf{\Pi}_p$ and $\mathbf{\Pi}_q$.

It can be easily proved that the three eigenvalues of $\mathbf{H}(\theta)$ are the products of those of $\mathbf{R}(\theta)$ with those of $\mathbf{H}_{pq}$, i.e., $(\mu, e^{i\theta}, e^{-i\theta})$. It can also be proved that the eigenvectors corresponding to $e^{\pm i\theta}$ are the imaged circular points $\mathbf{i}$, $\mathbf{j}$ and the one corresponding to μ traces out a conic by varying θ, which is the rotation conic as proved in the last Section.

From the properties of $\mathbf{H}_{pq}$ in (9), it can be easily derived that the above conclusions can be applied to planar patches. A translation + planar motion is proposed in which a patch performs an arbitrary translation followed by a motion on the patch plane. Note the patch can contain any pattern. An interesting example will be given in the next Section for a more intuitive illustration.

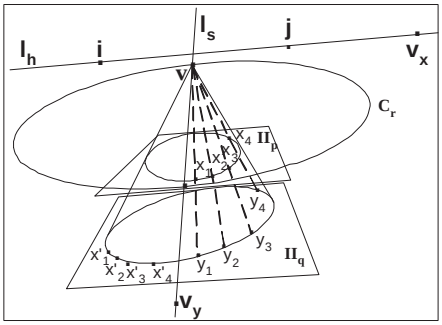

(a)

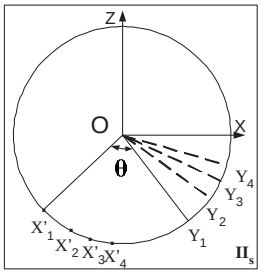

(b)

Figure 3. The homography constrained by the two conics. **(a)** The points x_i are mapped to points y_i by the homology $\mathbf{H}_{pq}$. **(b)** The points y_i and x'_i can be mapped to the points Y_i and X'_i on a unit circle with its center at the origin and with the same relative rotation angles.

4 Calibration with a Square Pattern

Squares are a common pattern in our daily life. A square can always have a circumcircle centered at the intersection of its two diagonals. Its four adjacent vertices $\mathbf{X}_1$, $\mathbf{X}_2$, $\mathbf{X}_3$ and $\mathbf{X}_4$ can be regarded as having a relative rotation of $\pi/2$ radians (see Fig.4(a)). These properties are exploited in the translation + planar motion for camera calibration.

Case I: from one square
Let $\mathbf{H}$ be the homography relating the images of the square vertices $\mathbf{X}_1$, $\mathbf{X}_2$, $\mathbf{X}_3$, $\mathbf{X}_4$ to $\mathbf{X}_4$, $\mathbf{X}_1$, $\mathbf{X}_2$, $\mathbf{X}_3$. This is the case in Section 3 when $X_i = X'_i$ and $Y_i = Y'_i$ $(i = 1, 2, 3, 4)$. Hence it can be easily derived that its eigenvectors are the image of the circle center $\mathbf{O}$ and the two circular points $\mathbf{i}$, $\mathbf{j}$ of the square plane. Since the image of the circle center does not provide constraints on ω, only $\mathbf{i}$, $\mathbf{j}$ give two constrains on ω. By viewing the square from at least three different orientations, a camera can be fully calibrated. Similarly at least two images are required for calibrating a zero skew/natural camera.

Case II: from two parallel squares
Consider two squares on parallel planes which have a rotation axis $\mathbf{l}_s$ through their centers and a translation along this axis(see Fig.4(b)). Let $\mathbf{H}$ be the homography relating the image of the two square vertices, i.e. $\mathbf{x}_1$, $\mathbf{x}_2$, $\mathbf{x}_3$, $\mathbf{x}_4$ to $\mathbf{x}'_4$, $\mathbf{x}'_1$, $\mathbf{x}'_2$, $\mathbf{x}'_3$. It can then be easily derived that the eigenvectors of $\mathbf{H}$ are the two circular points $\mathbf{i}$, $\mathbf{j}$ of the square plane and a point $\mathbf{v}(\theta)$ on the rotation conic $\mathbf{C}_r$, where $\mathbf{v}(\theta)$ corresponds to a rotation angle θ. Similarly other points on $\mathbf{C}_r$ can be obtained from the homography relating $\mathbf{x}_1$, $\mathbf{x}_2$, $\mathbf{x}_3$, $\mathbf{x}_4$ to $\mathbf{x}'_3$, $\mathbf{x}'_4$, $\mathbf{x}'_1$, $\mathbf{x}'_2$, and so on. From such correspondences, four points on $\mathbf{C}_r$ can be estimated. Together with the pair of imaged circular points $\mathbf{i}$, $\mathbf{j}$, the rotation conic $\mathbf{C}_r$ can be obtained. Hence the vanishing point $\mathbf{v}_y$ of the rotation axis can be obtained. Two more independent constraints on IAC given by

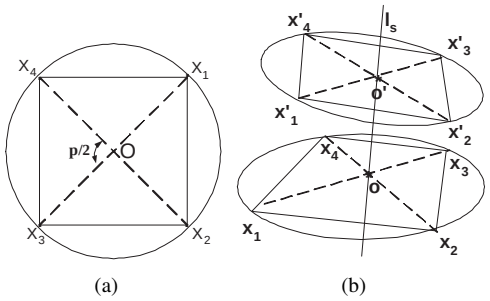

(a) (b)

Figure 4. Square patterns. **(a)** A square has a circumcircle and the vertices have relative rotation angles of $\pi/2$ radians. **(b)** Two equal squares have a vertical displacement and a rotation axis through their centers.

$$\mathbf{l}_h = \omega \mathbf{v}_y \tag{10}$$

can be obtained. Together with the constraints from the imaged circular points, there are four independent constraints on ω and thus a zero skew/natural camera can be calibrated. To fully calibrate the camera, at least two images taken from different camera orientations are necessary.

5 Experiments and Results

Since the camera calibration depends greatly on the calculation of the homography $\mathbf{H}(\theta)$, a pattern with N concentric squares (see Fig.7(a)) is thus designed to provide a better estimate of $\mathbf{H}(\theta)$. Synthetic and real experiments have been carried out to show the good precision of our approach.

5.1 Synthetic experiments

In the synthetic experiments, the camera has fixed intrinsic parameters, with focal length $f = 400$, aspect ratio $\alpha = 1.1$ and principle point at $(320, 240)$. The size of the calibration pattern is $20cm \times 20cm$. Gaussian noises of different levels were added to the points on the square edges. In the implementation, lines were fitted to the edge points and the square vertices were obtained as line intersections.

Single Square The first experiment was carried out on one square plane imaged from three different camera orientations with noise-free data and data with 15 different noise

levels from 0.1 pixels to 1.5 pixels. For each noise level, we performed 100 independent trials, and the results shown (see Fig.5(a)) are the average percentage errors of focal length, aspect ratio and principle point. From the figure we can see that errors increase linearly with the noise level.

In the second experiment, the camera was calibrated under different principle orientations with respect to the model plane. The orientations were chosen as a rotation angle of $\pi/6$ radians about a random axis in a unit sphere. In this experiment, the number of images used was between 2 and 15. For each number of images used, 100 trials of independent plane orientations and independent noise with zero mean and standard deviation of 0.5 pixels were conducted. The average result is shown in Fig.5(b). The errors decrease when more images are used. Note when only one image was given, the camera could not be calibrated. To have a good calibration, an even distribution of the principle direction should be provided so that the circular points will have an even distribution on the IAC.

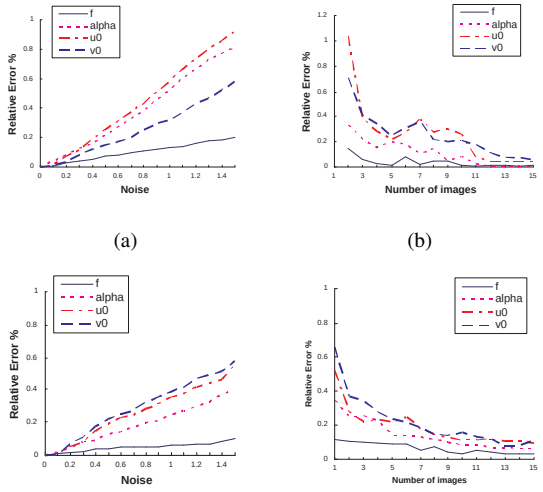

(a) (b)

(c) (d)

Figure 5. Relative errors of camera calibration. **(a)**With one square plane obtained under different noise levels. **(b)**With one square plane obtained under different number of images. **(c)**With two square planes obtained under different noise levels. **(d)**With two square planes obtained under different number of images.

Two Squares The corresponding experiments for calibration with two squares were also carried out to illustrate the effect of noise and number of different camera principle orientations. The distance between the two square planes was appropriately chosen so that no occlusion nor aliasing were present in the images. In the experiment a distance of half the largest square edge size was used. The rotation angle between the two squares was also chosen to ensure that the points on the rotation conic are scattered. A rotation angle of $\pi/4$ radians was used. Results are shown in Fig.5(c) and (d). Since in this case there were more constraints on calibration, the precision of camera calibration was improved compared with the case with only one square (Fig.5(a) and (b)). Note the calibration precision is greatly affected by the estimate of $\mathbf{v}_y$, hence we have to ensure $\mathbf{v}_y$ is not very far away. Note that an even distribution of rotation angle do not imply an even distribution of points on the rotation conic.

Due to the possible error in making the two-square pattern, two factors need to be tested. One is the distance d from the actual rotation axis to the assumed rotation axis, another is the relative angle ψ between the two square planes. In this experiment, we fix one of the two square planes and treat the normal line passing through this square center as the actual rotation axis. Then we set the largest d to be $1cm$ and the largest relative angle ψ be $\pi/12$ radians, and then divided them into 15 levels respectively. Given 3 images, the camera was calibrated under the image noise level of 0.5 pixel and the result is shown in Fig.6(a). We can see that the percentage error of camera parameters were within 1% if the errors of d and ψ were both under level 8, that is $d \leq 0.5cm$ and $\psi \leq \pi/24$, which is easy to be ensured in practise.

Comparison In this experiment, three different calibration methods were tested in parallel under the noise level of 0.5 pixel. The approach of calibration with one square and that with two squares were compared with the classical approach of Zhang [3] with one tessellated plane. Note the error of the x coordinate of principle point u_0 is the most distinct compared with those of all other parameters, thus in this experiment only the error of u_0 is used for illustration. From Fig.6(b), it can be concluded that the approach with two squares has a smaller error than the other two methods, which is because more constraints are exploited in each image. Note when the number of images used increases from 2 to 3, the errors of the classical approach and that of the method with one square decrease significantly, and similarly from 1 to 2, the error of the two squares approach decreases significantly.

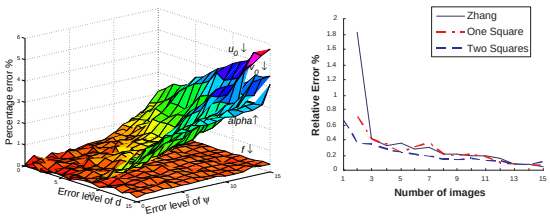

(a) (b)

Figure 6. Relative errors of the obtained camera parameters. **(a)** Under different error levels of making the two-square calibration pattern. **(b)** Comparison between different approaches under increased number of camera orientations.

5.2 Real Scene

In the real experiment, a Nikon100D CCD camera was calibrated by viewing the one and two square patterns. The image resolution is 1505×1000. The target has a general distance about 2m to the camera and has a size of $20cm \times 20cm$. It contains a pattern of 10 concentric squares, and hence 40 vertices. It was printed with a high-quality printer and put on a hard board. Images of the plane under different orientations were taken. The Canny edge detector[12] were then applied to find the points on the square edges, to which lines were fitted with a least square approach. The vertices are then detected as the intersection of the fitted straight lines.

Given 3 images taken under different plane orientations, the calibration methods with one and two parallel square patterns were compared with the non-linear refinement of that of Zhang [3]. The estimated parameters are listed in table 1, from which we can see that the approach with two squares is of a higher precision than the one with one square.

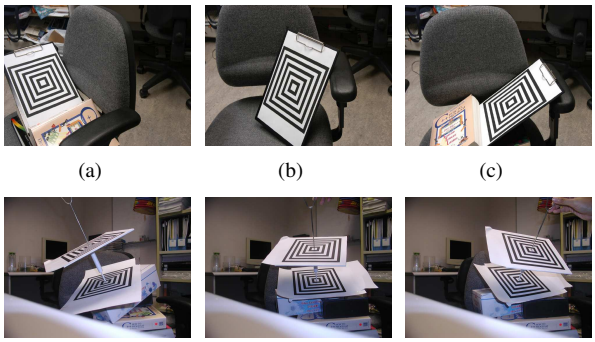

(a) (b) (c)

(d) (e) (f)

Figure 7. Real experiment. **Top row** Calibration with one pattern plane. **Bottom row** Calibration with two pattern planes.

Table 1. Estimated camera parameters with different approaches of camera calibration.

Settings	Focal Length	Aspect Ratio	Principle Point
Ground truth	2110.1	0.9986	(768.08, 542.48)
One square	2160.8	1.0078	(753.68, 492.16)
Two squares	2145.6	0.9967	(766.24, 522.74)

6 Conclusions

In this paper a novel translation + planar motion is proposed, under which the problem of camera calibration is studied by making use of the invariants under camera/object rotation. The homography and its eigenvectors relating the images before and after the motion are studied. By varying the relative rotation angles between the two point sets, the eigenvectors of the homography trace out a rotation conic which contains the images of the two circular points and the vanishing point of the rotation axis. A square pattern is then designed as a special application of the translation + planar motion. From the good precision of the results of both synthetic and real experiments, it can be seen that parallelism is not strictly required in the two-square case.

References

[1] Tsai R., "A versatile camera calibration technique for high accuracy 3d machine vision metrology using off-the-shelf tv cameras and lenses," *IEEE Journal of Robotics and Automation*, vol. 3(4), pp. 323–344, 1987.

[2] Sturm P. and Maybank S., "On plane-based camera calibration: A general algorithm, singularities, applications," in *Proc of CVPR, Fort Collins, USA*, 1999, pp. 432–437.

[3] Zhang Z., "A flexible new technique for camera calibration," *IEEE Trans. on PAMI*, vol. 22(11), pp. 1330–1334, 2000.

[4] Pollefeys M. and Gool V. L., "Stratified self-calibration with the modulus constraint," *Trans. on PAMI*, vol. 21(8), pp. 707–724, 1999.

[5] Hartley R.I., "Self-calibration of stationary cameras," *International Journal of Computer Vision*, vol. 22(1), pp. 5–23, 1997.

[6] Knight J., Zisserman A., and Reid I., "Linear auto-calibration for ground plane motion," in *Proc. IEEE Conf. on CVPR*, Jun 2003.

[7] Jiang G., Quan L., and Tsui H.T., "Circular motion geometry by minimal 2 points in 4 images," in *Proc. ICCV*, pp. 221–227.

[8] Beardsley P., Murray D., and Zisserman A., "Camera calibration using multiple images," in *Proc. of 2nd ECCV*, 1992, pp. 312–320.

[9] Faugeras O.D., Luong Q.-T., and Maybank S.J., "Camera self-calibration: Theory and experiments," in *ECCV92*, pp. 321–334.

[10] Hartley R.I. and Zisserman A., *Multiple View Geometry in Computer Vision*, Cambridge University Press, Cambridge, UK, 2000.

[11] Gentle J.E., *Numerical Linear Algebra for Applications in Statistics*, Springer-Verlag, Berlin, 1998.

[12] Canny J., "A computational approach to edge detection," *IEEE Trans. on PAMI*, vol. 8(6), pp. 679–698, 1986.